The Annual March of Heat Storage and Export in the Tropical Atlantic Ocean

STEFAN HASTENRATH

Department of Meteorology, University of Wisconsin, Madison, WI 53706

JACQUES MERLE

ORSTOM/LPDA, University of Paris VI, Paris, France

(Manuscript received 7 May 1985, in final form 30 September 1985)

ABSTRACT

The annual cycle and spatial patterns of subsurface heat storage Q_t and divergence of heat transport Q_v in the tropical Atlantic Ocean (30°N–20°S, east of 80°W) are studied on the basis of subsurface temperature soundings compiled until 1978 and evaluations of the net heat gain through the ocean surface ($Q_t + Q_v$) from long-term ship observations (1911–70). The net oceanic heat gain ($Q_t + Q_v$) follows in large part, but not exclusively, the annual cycle of insolation with largest gain in the respective summer, and loss in the winter half-year. The Q_t has an annual range and spatial gradients considerably larger than those of ($Q_t + Q_v$). Poleward of about 15°N, Q_t exhibits an annual cycle similar to ($Q_t + Q_v$) and insolation. By contrast, temporal and spatial variations of Q_t are more complicated in the equatorial Atlantic (about 10°N–10°S). For the average over this latitude band, heat depletion (negative Q_t) is found around March–May and largest storage around August–September. The divergence of oceanic heat transport Q_v is obtained as the difference between ($Q_t + Q_v$) and Q_t, and exhibits patterns broadly complementary to those of Q_t.

Calendar monthly maps indicate two major systems of annual cycle changes of Q_t. (i) A west–east seesaw variation is apparent in the equatorial belt (about 10°S–10°N), with heat depletion prevailing in the western equatorial Atlantic around March and April, and heat storage continuing in the Gulf of Guinea from January to around May. This heat budget pattern is associated with a deepening of isothermal surfaces to the west from about May to July, with a concomitant shallowing in the Gulf of Guinea. (ii) The zone 0–15°N is dominated by a northwestward shift of a band of negative Q_t from around March to August, and an inverse displacement thereafter. Both systems (i) and (ii) of seasonal changes in Q_t broadly parallel the annual cycle of the surface wind field over the tropical Atlantic, characterized by extrema around April and August.

1. Introduction

The tropical oceans are being increasingly recognized as an important component of the global climate system. The recent international documents on the World Climate Program (World Meteorological Organization, 1980, pp. 12–13, 39–41; World Meteorological Organization—ICSU, 1980, pp. 24–27; 1983, Vol. 1, pp. 1–20), in particular, draw attention to the fundamental role of the oceans in the storage and transport of heat, and the U.S. Five Year National Climate Plan (National Climate Program Office, 1980, pp. 46–50) declares research into ocean heat transport and storage a "principal thrust" required for understanding climate. Current field experiments (Anonymous, 1981a,b) include related objectives for limited regions.

Lamb and Bunker (1982) and Lamb (1981, 1984) have reviewed the work on the oceanic heat budget. Heat exchange processes across the sea-air interface have hitherto been studied most extensively (Budyko, 1963, 1974; Wyrtki, 1965, 1966; Hastenrath and Lamb, 1977, 1978, 1979; Bunker, 1976, 1980; Bunker and Worthington, 1976). By contrast, the storage of heat within the oceanic water body has received much less attention (Oort and Vonder Haar, 1976; Merle, 1980a,b; Barnett, 1981; Wyrtki and Uhrich, 1982; Levitus, 1982, 1984; Carissimo et al., 1985). "Direct" estimates of oceanic heat transport based on hydrographic sections are limited to a few transects (Bryan, 1962; Niiler and Richardson, 1973; Bennett, 1978; Bryden and Hall, 1980; Roemmich, 1980; Wunsch, 1980; Fu, 1981; Wunsch et al., 1983).

The global analysis of Levitus (1982, 1984) includes an evaluation of the annual cycle of heat storage in the Atlantic. For the tropical Atlantic, Lamb (1981) and Lamb and Bunker (1982) evaluated the hydrospheric storage and meridional transport of heat by 5 degree latitude bands. The net heat gain of the water body through the sea surface ($Q_t + Q_v$) was adopted from Hastenrath and Lamb (1978), the change in heat content Q_t was evaluated from subsurface observations, and the divergence of heat transport within the oceanic water body Q_v was obtained as the difference between the two aforementioned quantities. Meridional heat transports were derived from Q_v by spatial integration. Lamb and Bunker's (1982) study provides the first

comprehensive account of the annual march of hydrospheric heat storage and transport in the tropical Atlantic. The temporal resolution by bi-monthly intervals and the spatial resolution by 5 degree latitude bands across the width of the ocean are commensurate with the subsurface observations available for Lamb and Bunker's (1982) study.

In the meantime, a more extensive data base of subsurface observations has been compiled for the tropical Atlantic. This not only warrants a reappraisal of Lamb and Bunker's (1982) evaluations, but also invites the analysis of spatial patterns of subsurface heat budget terms, as well as a refinement of the annual cycle description. Results of this study are presented in this account and a forthcoming companion paper.

2. Observational data

Both surface and subsurface information are used in the present study. Evaluations of the surface heat budget based on long-term ship observations are available from earlier work (Hastenrath and Lamb, 1978), while for the subsurface conditions a new compilation of temperature profile observations is used.

The oceanic heat budget equation can be written

$$SW\Uparrow + LW\Uparrow + Q_s + Q_e = (Q_t + Q_v). \quad (1)$$

The left-hand terms denote, respectively, net shortwave and net longwave radiation, and sensible and latent heat transfer, terms being counted positive downward. The terms on the right are the storage and the divergence of lateral transport of heat within the oceanic water body. Hastenrath and Lamb (1978) evaluated the left-hand terms of Eq. (1) from long-term ship observations (1911–70) and thus obtained the net surface oceanic heat gain ($Q_t + Q_v$) as a residual. The calculations were made for all calendar months with a spatial resolution of one degree squares, but for purposes of the present study results were combined into two by four degree areas as shown in Fig. 1.

Subsurface temperature soundings in the tropical Atlantic between 30°N and 20°S and east of 80°W were compiled by the French Navy (Merle, 1983; Merle and Arnault, 1985). The data bank comprises 51 782 expendable bathythermograph (XBT), 93 525 mechanical bathythermograph (MBT) soundings, and 28 557 hydrocasts (station data), a total of 173 864 soundings. Most profiles stem from the U.S. National Oceanographic Data Center (NODC), but also included are additional XBT from the French Navy, Nansen CTD casts from the Oceanographic Vessel *Capricorne*, as well as soundings from various early expeditions, namely the *Meteor* in 1924, the *Atlantis* in 1931, the *Discovery* in 1935, the *Crawford* in 1957, and the *Equalant* in 1962–63, and GATE data. In general, the collections terminate in 1978. The distribution of observations is irregular in space and time. Data were processed by two degree latitude and four degree longitude areas as shown in Fig. 1. For each block, each calendar month, and each type of data (XBT, MBT, Nansen), soundings were evaluated in context. Profiles, which at any standard level showed temperature values departing by more than two standard deviations from the mean of all profiles, were rejected at all levels. For the area average profile, the three types of data were weighted according to the number of soundings retained. It is estimated that as a result the uncertainty of temperature values at each standard level is reduced to less than 0.1°C. However, for the regions of better coverage such as the Gulf of Guinea and the equatorial zone as a whole, and the layers outside the thermocline, the data are considered to be better than 0.05°C. Information was thus compiled for the standard depth 0, 5, 10, 20, 30, 40, 50, 60, 75, 100, 125, 150, 200, 250, 300, 400, 500 m, etc. Heat content was compiled for the layers bounded by these standard depths and the rectangular areas shown in Fig. 1., but only the layers from the surface to 100, 300 and 500 m are of interest here.

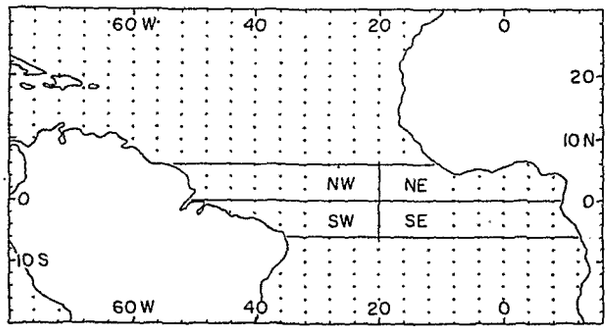

FIG. 1. Orientation map showing breakdown into rectangles of 2 degrees latitude by 4 degrees longitude. Boxes identified in the equatorial Atlantic refer to Fig. 7.

The spatial distribution of soundings is illustrated in Fig. 2, while the variation with depth is shown in Table 1. The density of observations broadly decreased southward and with depth. A substantial portion of the subsurface observations was obtained during 1971–78, and thus falls outside the aforementioned 1911–70 period of the surface ship observations. The frequency of subsurface soundings shows some variation in the course of the year, with minima in December–January, June and October, and maxima in March, August and November. Table 1 also compares the data volume of the present study with the publications of Robinson et al. (1979), Lamb and Bunker (1982), and Levitus (1982, 1984). Except for Robinson et al.'s (1979) atlas, the analysis of oceanic heat storage in these studies is confined to latitude-mean conditions. The present data compilation is considerably more plentiful than those of Levitus (1982, 1984), Lamb and Bunker (1982), and of Robinson et al. (1979) which moreover terminates at 150 m. The greatly improved data bank demonstrated by Table 1 is basic to the analysis of spatial

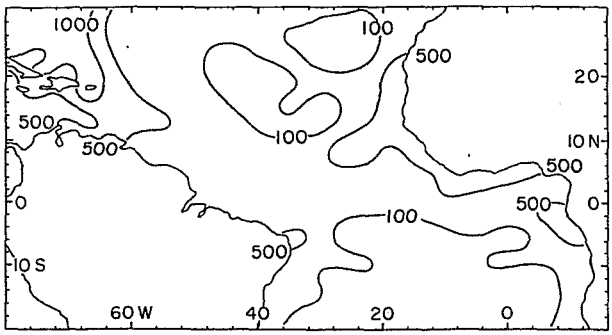

FIG. 2. Map showing number of soundings per rectangle (ref. Fig. 1).

patterns and the refinement in the description of the annual cycle.

3. Basic theory

Following Lamb and Bunker (1982), the heat storage in an oceanic column is given by

$$Q_t = \frac{\partial}{\partial t}\int_{z^*}^{0} \rho C_0 T dz$$

$$= (SW\!\uparrow\downarrow + LW\!\uparrow\downarrow + Q_s + Q_e) - Q_v \qquad (2)$$

where ρ, T and C_0 are the density, temperature and specific heat (constant volume) of sea water, respectively, z^* is the depth where the annual temperature variation vanishes, and other terms have their conventional meaning or are as defined for Eq. (1).

In the present study, calendar monthly values of Q_t are estimated from the long-term subsurface temperature data described in Section 2. For each 2 by 4 degree rectangular area (Fig. 1) the heat content of layers is calculated from the temperature at standard depths using the trapezoidal rule, formally analogous to the integral in Eq. (2); of interest being the layers surface to 100, 300 and 500 m depth. Then the storage, or rate of change in heat content, is estimated for each month. This is approximated by the difference of heat content of the following minus that of the preceding month divided by the time interval Δt of two months.

Subtraction of the monthly subsurface heat storage Q_t from the net surface heat gain $(Q_t + Q_v)$ formally yields an estimate of the divergence of lateral heat transport within the ocean Q_v. Depending on the depth to which Q_t is calculated, somewhat different values of Q_v are obtained.

Integration of Q_v with latitude yields meridional heat transport, given a transport value at, say, the southern boundary. Inasmuch as no new estimates for the extratropics are obtained here, no improvement over Lamb and Bunker's (1982) transport computations can be offered, although the comparison of Q_v values for the tropics appears appropriate. Note, however, that at the northern boundary of the present analysis, 30°N, area coverage does not extend across the whole width of the ocean.

It is difficult to assess uncertainties in estimating the various heat budget terms. Concerning the net surface heat gain $(Q_t + Q_v)$, uncertainties are estimated to be more than 20 W m^{-2}, based on the propagation of errors in the directly calculated surface heat budget components (net short and longwave radiation, latent and sensible heat fluxes), as explained in Hastenrath and Lamb (1978, p. vii). Given the uncertainties in estimating the uncertainties of estimates, this amount should not be regarded as inconsistent with the somewhat larger values proposed by Weare et al. (1981) and Reed (1983).

The oceanic heat storage is calculated from the difference in heat content at bi-monthly intervals. As indicated in Section 2, for most of the oceanic column and for much of the area analyzed, the temperature uncertainty is less than 0.05°C. This corresponds to an uncertainty in heat content of the column surface to 500 m depth of 10^8 J m^{-2}, and according to the law of random error propagation to an uncertainty of $\sqrt{2} \times 10^8$ J m^{-2} for the difference in heat content between two reference times. The time interval between reference times is here about 5×10^6 s. This results in an uncertainty of heat storage (rate of change in heat content) of about 30 W m^{-2}. Errors are compounded in Q_v, obtained as the difference between $(Q_t + Q_v)$ and Q_t. The aforementioned uncertainties are mitigated by averaging over latitude bands. However, in the monthly maps of heat budget terms (Figs. 4–6), characteristics of (relative) spatial patterns and annual cycle must be regarded as more informative than absolute values.

TABLE 1. Comparison of number of soundings (in 10^2) available in present study, H + M, with Lamb and Bunker (1982), La + Bu, Robinson et al. (1979), RBS, and Levitus (1982, 1984), Le. Note that in Robinson et al. (1979) the analysis is to a depth of 150 m only.

	H + M				La + Bu			RBS		Le		
	0	100	300	500	0	100	500	0	150	0	100	500 m
30–20°N	750	745	285	236	238	205	(60)	279	150	487	477	34
20–10	404	394	185	117	180	150	(35)	199	114	353	317	39
10°N–0	336	303	142	105	68	48	15	98	70	181	149	30
0–10°S	185	166	67	39	49	39	11	(43)	(33)	123	113	21
10–20	62	60	30	15	27	25	5			57	54	10
30°N–20°S	1,738	1,667	709	512	552	467	126	(619)	(367)	1,201	1,110	134

Uncertainties in estimates of meridional heat transport have been considered by Lamb and Bunker (1982). Possible independent errors of 15 W m^{-2} in $(Q_t + Q_v)$ and Q_t, and of 5×10^{13} W in the heat transport across an initial latitude boundary accumulate into uncertainties up to the order of 100×10^{13} W for the heat transport across various latitude circles.

4. Latitude-mean conditions

The purpose of this section is to offer a framework for the more detailed discussion of spatial patterns in Section 5, and to provide a check of the latitude-mean analysis of Lamb and Bunker (1982).

The annual march of the hydrospheric heat storage in the layers surface to 100, 300 and 500 m, was evaluated for 2 degree latitude bands, but only plots for 6 degree latitude zones are shown in Fig. 3. Lamb and Bunker's (1982) graphs with a bi-monthly time resolution and for 5 degree latitude belts are consistent with Fig. 3 in all major respects. The annual variation tends to decrease from the higher latitudes equatorward, but is remarkably large in the equatorial region. It is further noteworthy that in the latitude bands equatorward of 12°N and S, Q_t shows little resemblance to the annual march of insolation. The annual range of Q_t amplifies greatly from 100 to 300 m, while the curves for 300 and 500 m are similar. A detailed documentation of Q_t with respect to the 300 and 500 m levels is available in Table 2, parts b and d. The comparison between layers shows consistency with time and depth, and indicates that the analysis to the depth of 500 m is warranted. Accordingly, that lowest level is considered in the following discussion and the map representation in Figs. 6 and 8.

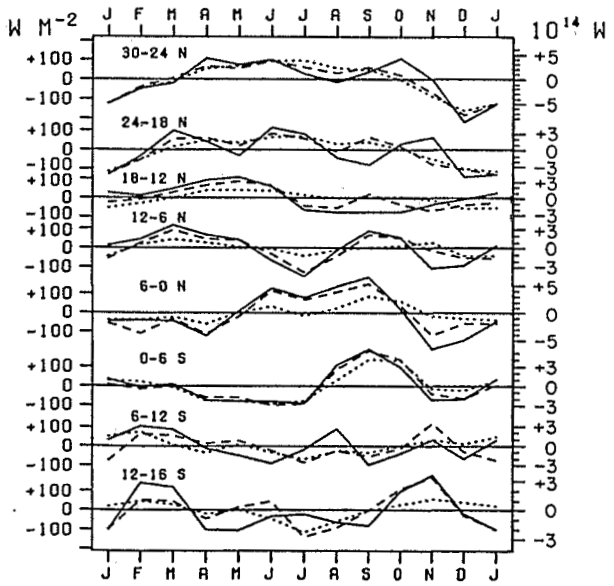

FIG. 3. Annual march of rate of subsurface heat storage (Q_t) within 6 degree latitude zones of the tropical Atlantic. Dotted, broken, and solid lines refer to the top 100, 300 and 500 m of ocean, respectively. The left-hand scale pertains to area averages in W m^{-2}, and the right-hand scale to sums over latitude strips in 10^{14} W.

Three quantities related to the oceanic heat budget are to be considered in context: the net surface heat gain $(Q_t + Q_v)$; the heat storage within the hydrospheric column Q_t; and the divergence of the lateral heat transport in the ocean Q_v, which is obtained as the difference between the former two quantities. Diagrams showing the latitudinal and annual variation of $(Q_t + Q_v)$, Q_t, and Q_v, expressed per unit area, are presented in Fig. 4. Table 2 lists the heat budget terms $(Q_t + Q_v)$, Q_t, and Q_v, integrated over the entire area of the respective latitude bands. Values of Q_t, and correspondingly also of Q_v, are given as calculated with respect to the 500 and 300 m levels.

The diagram of $(Q_t + Q_v)$ in part A of Fig. 4 is essentially the same as shown in Hastenrath (1977) and Lamb and Bunker (1982). In the equatorial region, there is a net surface heat gain throughout the year, while further away from the equator heat gain/loss prevails in the respective summer/winter season.

The diagram of oceanic heat storage Q_t with respect to 500 m depth shown in part B of Fig. 4 details the latitudinal pattern of annual cycle characteristics shown in Fig. 3. In the zones poleward of about 15°N and S, heat storage/depletion predominates during the respective summer/winter half-years, in some similarity to the behavior of $(Q_t + Q_v)$ as displayed in part A of Fig. 4. However, as mentioned above in relation to Fig. 3, the pattern becomes more complicated in the equatorial region to the North of the equator (about 0–6°N); heat depletion is largest around March–April, and storage around June–September. In the zone immediately South of the equator extrema occur somewhat later, namely around April–June and August–October.

In all major respects and for all latitude belts, Fig. 4 is consistent with the results of Lamb and Bunker (1982, Table 3). However, the analysis presented in Section 5, and the maps in Fig. 6 adds information on the spatial distribution and the zonal contrasts contained in the latitude-mean pattern. Figures 3 and 4 should also be compared with Merle's (1980a, Figs. 5 and 8) study for the equatorial zone (6°N to 6°S) of the Atlantic, which has recently been substantiated further by Houghton's (1983) analysis for the Gulf of Guinea. Merle (1980a,b) finds a broadly inverse variation of oceanic heat content in the layer surface to 300 m between the western and eastern part of the equatorial Atlantic, with a considerably larger annual range in the west. Thus the annual cycle in the western equatorial Atlantic dominates the zonal average conditions, by prevailing over the broadly inverse annual cycle in the east. The zonal average conditions are thus characterized by a smallest/largest heat content around May–June/October–November and a general phase lag southward. The aforementioned features of the annual

TABLE 2. Monthly means of oceanic heat budget terms for latitude zones of the tropical Atlantic, in 10^{13} W. (a) net surface heat gain ($Q_t + Q_v$); (b) heat storage in layer surface to 500 m depth, Q_{t500}; (c) divergence of lateral heat transport within the ocean, calculated with respect to the 500 m level, Q_{v500}; (d) heat storage in layer surface to 300 m depth, Q_{t300}; (e) divergence of lateral heat transport within the ocean, calculated with respect to the 300 m level, Q_{v300}.

	J	F	M	A	M	J	J	A	S	O	N	D	Year
(a) $(Q_t + Q_v)$													
30–28°N	−16	−10	−3	+5	+11	+14	+13	+9	+3	−7	−16	−18	−1
28–26	−14	−8	−1	+5	+10	+14	+11	+9	+4	−4	−14	−16	−0
26–24	−12	−6	+1	+5	+9	+12	+9	+7	+4	−2	−12	−16	−0
24–22	−12	−5	+1	+5	+8	+10	+7	+6	+3	−1	−11	−14	−0
22–20	−11	−4	+2	+5	+8	+7	+4	+4	+3	−1	−8	−13	−0
20–18	−9	−3	+2	+5	+6	+6	+3	+3	+3	−1	−6	−11	−0
18–16	−9	−3	+3	+5	+6	+4	+3	+3	+3	−1	−6	−12	−0
16–14	−8	−3	+2	+5	+5	+3	+3	+4	+3	−0	−5	−10	−0
14–12	−6	−2	+3	+5	+4	+3	+4	+4	+5	+1	−4	−8	+1
12–10	−5	−1	+3	+4	+3	+2	+3	+4	+5	+2	−2	−6	+1
10–08	−3	−1	+2	+2	+1	+1	+2	+2	+4	+2	−1	−4	+1
8–06	−2	−1	+2	+2	+1	+1	+1	+1	+3	+4	+1	−1	+1
6–04	+2	+3	+4	+3	+1	+0	+0	+1	+3	+5	+4	+2	+2
4–02	+5	+5	+4	+3	+1	−1	−1	+2	+4	+5	+4	+4	+3
2°N–0	+6	+7	+6	+5	+3	+2	+3	+4	+5	+6	+5	+4	+5
0–02°S	+8	+9	+8	+6	+5	+7	+8	+9	+9	+7	+6	+7	+7
2–04	+8	+9	+7	+4	+3	+5	+7	+7	+8	+6	+5	+6	+6
4–06	+7	+8	+6	+3	−0	−0	+1	+3	+5	+4	+5	+5	+4
6–08	+7	+8	+5	+1	−3	−5	−5	−1	+3	+3	+4	+5	+2
8–10	+6	+7	+4	−0	−5	−8	−8	−4	+0	+2	+4	+4	+0
10–12	+6	+8	+3	−1	−6	−9	−10	−6	−2	+1	+3	+4	−1
12–14	+6	+7	+3	−1	−6	−8	−9	−6	−1	+1	+4	+5	−0
14–16	+7	+7	+3	−1	−6	−8	−8	−5	−1	+3	+5	+5	+0
16–18	+8	+7	+3	−1	−5	−8	−7	−3	−0	+4	+6	+7	+1
18–20°S	+10	+7	+3	−2	−7	−8	−8	−2	−0	+4	+8	+8	+1
(b) Q_{t500}													
30–28°N	−21	−4	−15	+19	+21	+12	+6	+0	+8	+23	+2	−32	+2
28–26	−14	−6	+5	+11	+8	+15	+9	−2	+6	+24	−5	−34	+2
26–24	−17	−9	+2	+17	+14	+14	−4	+5	+3	−3	+2	−25	−0
24–22	−21	−9	+16	+1	+3	+18	+11	+7	−16	+0	+16	−22	+0
22–20	−23	+3	+20	+6	+0	+12	+9	−11	−8	+11	+13	−26	+1
20–18	−10	−6	+8	+10	+2	+17	+14	−13	−8	+3	−1	−13	+0
18–16	−0	−0	+10	+15	+7	−1	+11	+3	−15	−16	−5	+5	+1
16–14	+8	+2	+7	+8	+21	+28	−15	−19	−4	−23	−5	+4	+1
14–12	+5	+4	+5	+19	+21	−1	−15	−17	−2	+6	+7	−12	+2
12–10	−0	+7	+13	+30	+20	−13	−27	−17	−6	+18	−2	−16	+0
10–08	+7	+10	+21	+10	−3	−15	−24	−3	+3	−5	−5	+4	+0
8–06	−2	+1	+8	−15	−2	+4	−4	+16	+34	+7	−3	−13	+3
6–04	−1	−6	−13	−20	+3	+28	+27	+15	+9	+6	−7	−22	+2
4–02	−13	−13	−6	−13	+10	+24	+10	+19	+38	−3	−12	−17	+2
2°N–0	−2	+4	+3	−16	−9	+2	−6	+22	+42	+5	−32	−17	−0
0–02°S	+9	+2	+3	−9	−19	−20	−10	+23	+39	+20	−23	−17	−0
2–04	+2	−6	−0	−10	−12	−3	−4	+5	+19	+20	−5	−9	−0
4–06	+3	+2	+2	−8	+1	−6	−20	+13	+13	−4	+1	+1	−0
6–08	−0	−3	+3	−2	−1	−12	+6	+32	−12	−5	+4	+3	+1
8–10	+9	+17	+13	+3	−3	−15	−13	−1	−8	+6	+1	−10	+0
10–12	+4	+24	+16	−5	−13	−4	+1	+2	−14	−2	+8	−16	+0
12–14	−12	+16	+17	−8	−16	−3	+0	−7	−11	+11	+22	−4	+1
14–16°S	−13	+19	+12	−17	−9	−4	−5	−5	−9	+12	+23	−0	+0
(c) Q_{v500}													
30–28°N	+5	−6	+13	−14	−10	+2	+6	+9	−5	−30	−18	+14	−3
28–26	−0	−2	−6	−6	+3	−1	+2	+12	−2	−28	−10	+17	−2
26–24	+5	+2	−2	−12	−5	−2	+13	+3	+1	+1	−14	+9	−0
24–22	+10	+5	−15	+5	+5	−9	−4	−1	+20	−1	−26	+7	−0
22–20	+12	−7	−18	−1	+7	−5	−5	+15	+11	−12	−21	+13	−1
20–18	+1	+3	−5	−5	+4	−11	−11	+16	+11	−4	−6	+2	−0
18–16	−9	−3	−7	−10	−1	+5	−8	+0	+18	+15	−1	−17	−1
16–14	−16	−5	−5	−2	−16	−25	+18	+23	+7	+23	+1	−14	−1

TABLE 2. (*Continued*)

	J	F	M	A	M	J	J	A	S	O	N	D	Year
14–12	−11	−6	−2	−14	−16	+3	+18	+21	+7	−5	−11	+4	−1
12–10	−5	−7	−9	−26	−16	+15	+30	+22	+11	−16	+0	+11	+1
10–08	−10	−11	−19	−8	+4	+16	+25	+5	+1	+7	+4	−7	+1
8–06	+0	−1	−6	+17	+3	−3	+5	−16	−30	−3	+4	+12	−2
6–04	+3	+8	+17	+23	−2	−28	−26	−14	−6	−1	+10	+25	+1
4–02	+18	+18	+10	+16	−9	−25	−11	−17	−34	+7	+16	+21	+1
2°N–0	+8	+3	+3	+21	+12	+1	+9	−18	−37	+1	+38	+21	+3
0–02°S	−1	+7	+5	+15	+24	+27	+17	−15	−31	−13	+29	+24	+7
2–04	+6	+14	+8	+14	+15	+8	+11	+3	−11	−13	+10	+15	+6
4–06	+4	+5	+5	+10	−2	+6	+21	−10	−8	+8	+4	+4	+4
6–08	+7	+11	+3	+3	−2	+7	−11	−32	+15	+8	+0	+3	+1
8–10	−12	−20	−15	−4	+4	+16	+13	+1	+7	−8	−4	+6	−1
10–12	−13	−29	−19	+6	+16	+8	+3	+1	+14	−3	−18	+4	−2
12–14	+6	−19	−17	+11	+20	+6	+3	+9	+12	−12	−27	−3	−1
14–16°S	+12	−19	−11	+17	+9	+5	+6	+6	+9	−12	−24	−2	−0
(d) Q_{t300}													
30–28°N	−18	−2	−1	+5	+10	+12	+15	+4	+8	+2	−12	−23	−0
28–26	−14	−7	+1	+11	+6	+13	+10	+4	+5	+9	−8	−30	+0
26–24	−20	−7	+5	+14	+9	+13	+2	+4	+13	−2	−9	−23	−0
24–22	−21	−6	+8	+7	+5	+11	+9	+9	+4	−5	−6	−16	−0
22–20	−19	−4	+11	+11	−1	+7	+6	−5	+15	+11	−12	−19	+0
20–18	−15	−11	+5	+9	+5	+18	+10	−9	+8	+1	−13	−9	−0
18–16	−7	−3	+7	+8	+6	+3	+7	+5	+3	−9	−14	−2	+0
16–14	+2	+0	+3	+5	+15	+25	−9	−12	+1	−13	−11	−6	+0
14–12	−6	−0	+4	+17	+18	+2	−7	−16	+6	+6	−5	−9	+1
12–10	−8	+5	+11	+17	+19	−2	−28	−22	−1	+17	+4	−15	−0
10–08	−2	+8	+18	+12	−0	−12	−19	−7	−0	−5	+4	+5	+0
8–06	−10	−3	+4	−13	−4	+3	+0	+14	+25	+7	−4	−8	+1
6–04	−6	−17	−11	−17	−3	+26	+27	+10	−4	+5	+0	−8	+0
4–02	−14	−20	−4	−13	+7	+25	+7	+19	+31	−1	−9	−9	+2
2°N–0	−2	−5	+4	−15	−11	−3	−6	+16	+38	+11	−24	−5	−0
0–02°S	+10	−1	−1	−9	−17	−22	−13	+17	+40	+28	−19	−14	−0
2–04	−2	−5	+1	−9	−13	−3	−2	+4	+21	+23	−5	−12	−0
4–06	−5	+1	−1	−3	+7	−11	−20	+12	+9	−0	+9	+2	−0
6–08	−11	−0	+3	+5	+5	−11	−1	+14	−12	−9	+16	+2	+0
8–10	−8	+10	+9	+6	+5	−5	−16	−14	−4	+6	+14	−3	+0
10–12	−7	+14	+9	−5	+1	+9	−13	−7	−3	−1	+14	−9	+0
12–14	−13	+6	+8	−4	+1	+7	−16	−8	+2	+8	+20	−4	+1
14–16°S	−11	+7	+4	−7	+3	+2	−17	−8	−2	+17	+23	−3	+1
(e) Q_{v300}													
30–28°N	+2	−8	−1	+1	+1	+2	−2	+5	−5	−8	−4	+5	−1
28–26	−0	−2	−2	−6	+5	+0	+2	+6	−1	−13	−6	+14	−0
26–24	+8	+1	−4	−9	+0	−2	+8	+4	−9	−0	−4	+7	−0
24–22	+9	+1	−7	−1	+3	−1	−2	−4	−1	+4	−5	+2	−0
22–20	+8	+0	−10	−6	+9	+1	−1	+9	−13	−12	+4	+7	−0
20–18	+6	+8	−2	−4	+1	−13	−7	+13	−5	−2	+7	−2	−0
18–16	−3	+0	−4	−3	−1	+1	−4	−2	+0	+8	+8	−10	−0
16–14	−10	−3	−1	+0	−10	−22	+12	+16	+2	+12	+7	−4	−0
14–12	−0	−2	−1	−13	−13	+1	+10	+21	−1	−5	+1	+1	−0
12–10	+3	−5	−8	−13	−15	+4	+31	+26	+6	−15	−6	+10	+1
10–08	−2	−9	−16	−10	+1	+13	+21	+9	+4	+7	−4	−8	+1
8–06	+8	+2	−2	+15	+6	−2	+1	−13	−22	−3	+5	+7	+0
6–04	+8	+20	+15	+20	+4	−26	−27	−9	+8	+0	+3	+10	+2
4–02	+19	+25	+8	+16	−6	−26	−8	−17	−27	+5	+12	+12	+1
2°N–0	+8	+13	+2	+20	+14	+5	+10	−12	−32	−5	+29	+9	+5
0–02°S	−2	+10	+9	+15	+22	+29	+21	−9	−31	−21	+26	+21	+7
2–04	+9	+14	+6	+13	+16	+8	+9	+4	−13	−17	+10	+18	+6
4–06	+12	+7	+7	+6	−7	+11	+20	−8	−4	+5	−4	+4	+4
6–08	+18	+8	+3	−4	−8	+6	−4	−14	+15	+12	−12	+3	+2
8–10	+5	−13	−11	−6	−4	+6	+16	+14	+3	−8	−17	−1	−1
10–12	−2	−19	−12	+6	+2	−5	+17	+10	+3	−3	−24	−3	−2
12–14	+8	−8	−7	+7	+3	−3	+19	+10	−1	−9	−25	−3	−0
14–16°S	+10	−7	−3	+8	−2	−1	+18	+10	+3	−17	−24	+1	−0

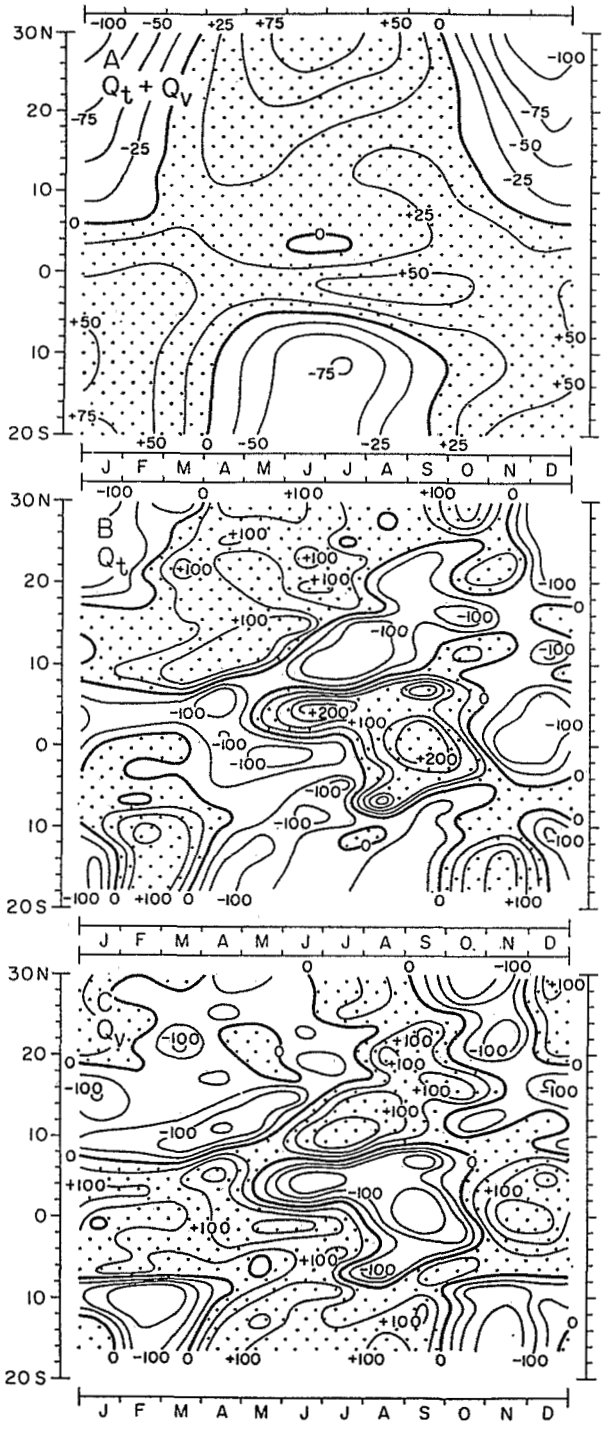

FIG. 4. Latitudinal and annual variation of oceanic heat budget. (A) net surface heat gain ($Q_t + Q_v$); (B) heat storage in the layer surface to 500 m Q_{t500}; (C) divergence of heat transport, calculated with reference to the 500 m level, $Q_{v500} = (Q_t + Q_v) - Q_{t500}$. Quantities are in W m^{-2}, zero line is heavy, and dot raster denotes positive areas.

march of heat content identified by Merle (1980a,b) are in accordance with the prominent Q_t variations apparent in the present Figs. 3 and 4, namely the largest heat depletion (negative Q_t) around March/April in the North equatorial Atlantic, and around April–June in the South equatorial waters, as well as with the largest heat storage (positive Q_t) around May–July to the North and around August–September to the South of the equator. The opposition of phase between the western and eastern equatorial Atlantic pointed out by Merle (1980a,b) is further of interest in relation to the spatial patterns of Q_t to be discussed in Section 5. Figure 4, part B, also shows a northward migration of a zone of heat depletion, from around 5°N during January–April to 15–20°N around August–September, and a subsequent southward shift, broadly paralleling the annual cycle of the surface wind field and the variation of ocean current systems.

The diagram of the divergence of oceanic heat transport Q_v in part C of Fig. 4 results as difference between the isopleth plots in parts A and B, and shows a pattern broadly inverse to the heat storage Q_t (part B). There is an overall tendency towards smaller divergence or even convergence of heat transport as one proceeds poleward. However, the pattern is complicated in the equatorial region (between approximately 10°N and S), where divergence of heat transport prevails during much, but not all of the year. Particularly striking is the large heat transport convergence during May–October to the North of the equator, and around August–September in the South equatorial waters. Merle (1983) has related these heat budget features to annual cycle displacements of the thermocline, and Merle and Arnault (1985) further analyzed the seasonal characteristics of surface dynamic topography in the tropical Atlantic.

Figure 4 illustrates that in the equatorial zone neither the heat storage Q_t nor the heat transport divergence Q_v show any similarity to the annual cycle of insolation—in contrast to the pattern of the net surface heat gain ($Q_t + Q_v$). In fact, the major controls for the annual variation of Q_t and Q_v in the equatorial region must be sought for the dynamics of the upper ocean. Similar suggestions have been offered before by Merle (1980a,b) and Levitus (1984). Ocean dynamics affect the heat budget of the upper hydrosphere in various ways. Mixed-layer behavior and characteristics of the thermocline will be discussed in a forthcoming companion paper.

The meridional heat transport within the oceanic water body can be evaluated from Q_v only given a transport value at the northern or southern boundary of the Atlantic domain. Such computations have been presented by Hastenrath (1980, 1982) for annual mean conditions. Based on their analysis for the entire North Atlantic, Lamb and Bunker (1982) were for the first time able to produce transport estimates for bi-monthly intervals at various latitudes of the North and tropical Atlantic. For comparison with their results it may appear attractive to adopt their value for 30°N, the northern limit of our domain, and integrate southward.

However, this is not feasible because our analysis extends westward only to 80°W, while Lamb and Bunker's (1982) values refer to the entire latitude circle from coast to coast. Therefore, we adopted their transport value for 10°S and integrated northward. The meridional heat transports resulting from the Q_v values of the present study as shown in Fig. 4, part C, and Table 2, part C are listed for selected latitudes in Table 3. Overall, the heat transport estimates are similar to Lamb and Bunker's (1982), not only because their value for 10°S was adopted, but also because the Q_v values in the present Fig. 4 and Table 2 and in Lamb and Bunker (1982) agree closely in both general magnitude and characteristics of the annual cycle. Northward of 10°N the differences beween our and Lamb and Bunker's (1982) values become larger, presumably in large part due to the fact that our analysis extends westward only to 80°W rather than over the entire width of the ocean. Zonal transports across the western boundary of our domain, between 10 and 30°N are thus not accounted for.

5. Spatial patterns

The net surface heat gain $(Q_t + Q_v)$, the heat storage from surface to 500 m depth Q_{t500}, and the divergence of lateral heat transport in the ocean Q_{v500}, are mapped in Figs. 5, 6 and 8. Expanding on the latitude average diagrams, Fig. 4, the maps of Figs. 5, 6 and 8 describe the major spatial patterns.

The maps of net surface heat gain $(Q_t + Q_v)$ for December through February (Fig. 5, parts L, A, B) show large heat losses in the outer tropics of the Northern Hemisphere, but gains in most of the equatorial and South Atlantic. Proceeding from March towards July and August (Fig. 5, parts C to H), the heat loss in the northern portion of the map area gradually gives way to substantial gain, while the inverse development takes place in the South Atlantic. Similarly, from September to February (Fig. 5, parts I to L, and A, B) the map sequence is characterized by changes to increasing heat loss in the North, and heat gain in the equatorial and South Atlantic. The annual variation of the spatial patterns of $(Q_t + Q_v)$ thus appears, in large part but not exclusively, understandable from the annual cycle of solar forcing. A prominent exception is the evolution in Northern summer of a tongue of maximum heat gain in the eastern Atlantic immediately to the south of the equator, contrasting with a band of heat loss to the north of it. This is directly related to the development of a cold water tongue and reduced evaporation to the south of the eastern Atlantic equator (Hastenrath, 1978) and thus presumably to the vertical motion field of the equatorial ocean. Likewise the cold water upwelling regime off the coast of Northwest Africa stands out as a region of large net oceanic heat gain. By contrast, the interior of the tropical North Atlantic exhibits a net oceanic heat loss for the year as a whole (Hastenrath and Lamb, 1978, chart 83), a feature explained by Behringer and Stommel (1981) from the dynamics of the upper hydrosphere. However, at least the major hemispheric characteristics of the annual variation of $(Q_t + Q_v)$ appear plausible from the annual cycle of solar forcing. As was already pointed out with reference to Fig. 4, this is not the case for Q_t and Q_v.

Maps of oceanic heat storage Q_t were constructed for the layers from the surface to 100, 300, and 500 m depth. These demonstrate an overall consistency of the major pattern characteristics with depth. Only the charts for oceanic heat storage Q_t with reference to 500 m depth are reproduced here as Fig. 6. The maps are noisy and are intended to give a first and preliminary orientation on the major pattern characteristics, whereas discussion of details does not appear warranted.

For the outer tropics of either hemisphere, the maps of oceanic heat storage Q_t presented in Fig. 6 exhibit an annual cycle similar to $(Q_t + Q_v)$ or the annual march of insolation, while the pattern sequence is more complicated in the equatorial region. Thus in the Q_t maps for December to February (Fig. 6, parts L, A, B) heat depletion (negative Q_t) is indicated for much of the North Atlantic poleward of about 15°N, and a tendency for heat storage in the South Atlantic waters. Proceeding from March toward July (Fig. 6, parts C to G), the prevalence of heat depletion in the northern portion of the map area gives way to heat storage, while heat depletion becomes more prominent in the South Atlantic.

The annual cycle of Q_t is distinctly different equatorward of about 15 degrees latitude. Pronounced pattern changes take place from March to July and August (Fig. 6 parts C to L). Two major systems of annual cycle changes stand out, namely (i) a "teeter-totter" variation in the zonal direction in the equatorial belt,

TABLE 3. Bi-monthly values of "vertically and zonally integrated net meridional heat transport" across selected latitudes of the tropical Atlantic, calculated with respect to the 500 m depth level in 10^{13} W, positive northward. (a) from Lamb and Bunker (1982); (b) present study.

	JF	MA	MJ	JA	SO	ND	Year
(a) La + Bu							
30°N	+124	+57	+164	+174	+215	−106	+107
20	+138	+85	+170	+195	+226	−148	+114
10°N	+127	+156	+118	+192	+245	−181	+112
0	+78	+163	+61	+203	+294	−208	+101
10°S	+76	+108	+35	+194	+318	−255	+81
(b) H + M							
30°N	+87	+96	+36	+254	+260	−169	+98
20	+75	+124	+44	+229	+282	−154	+101
10°N	+104	+167	+73	+164	+248	−139	+106
0	+86	+130	+87	+193	+295	−209	+99
10°S	+76	+108	+35	+194	+318	−255	+81

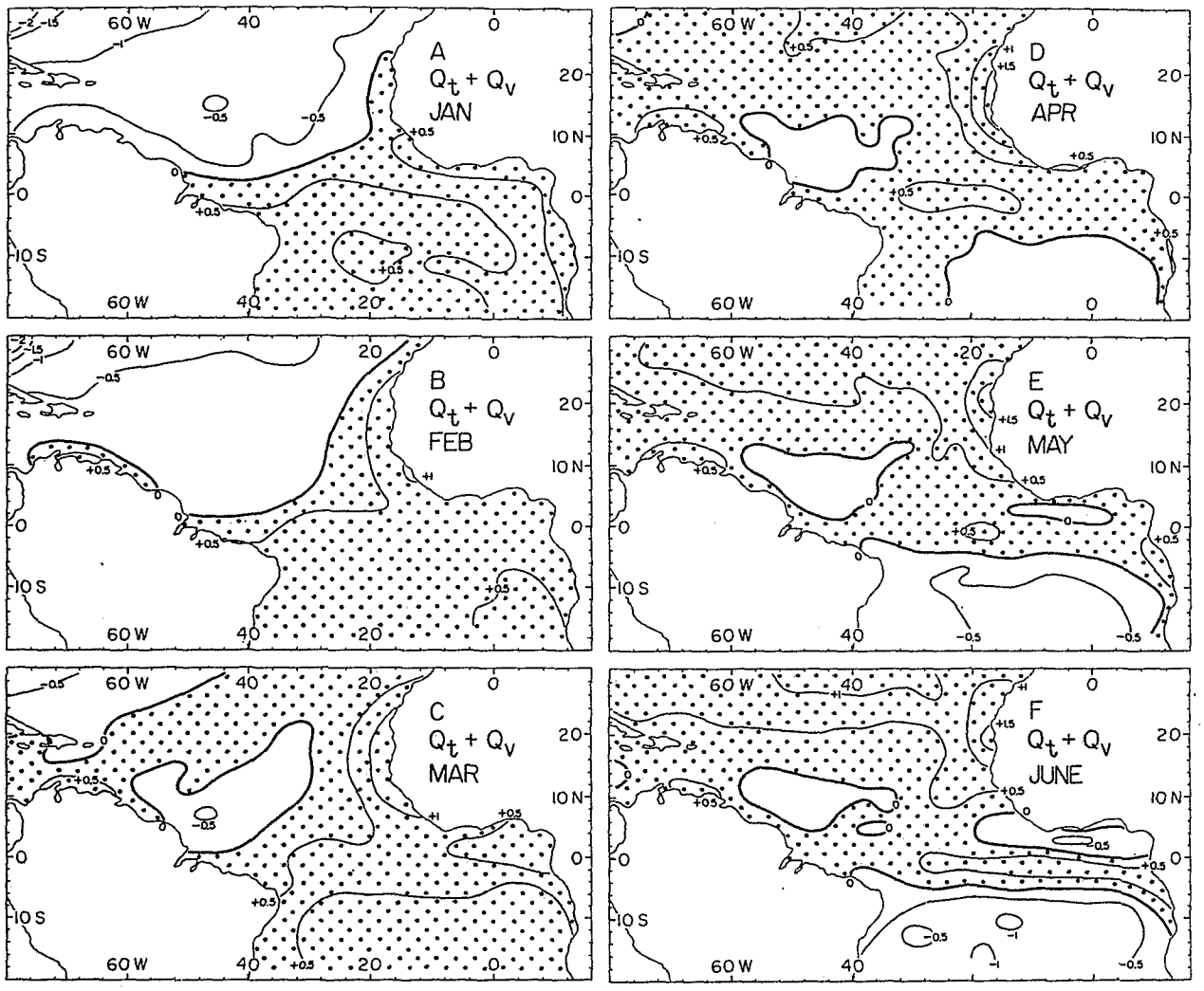

FIG. 5. Monthly maps of net surface heat gain ($Q_v + Q_t$) for (A) January, (B) February, (C) March, (D) April, (E) May and (F) June. Figure 5 (continued) (G) July, (H) August, (I) September, (J) October, (K) November and (L) December. Quantities are in 10^2 W m^{-2}, zero line is heavy, and dot raster denotes positive areas.

and (ii) a meridional shift of patterns in the low-latitude North Atlantic. Only these two most prominent systems of annual pattern variation are considered in the following.

Concerning the first (i) of these large-scale systems, attention is called to the equatorial zone (about 10°N to 10°S) of the Atlantic. The map sequences in Fig. 6 adds spatial detail to the earlier findings of Merle (1980a, Figs. 5, 8). In the western equatorial Atlantic, heat depletion (negative Q_t) prevails around March and April (Fig. 6, parts C and D), while in the Gulf of Guinea heat storage (positive Q_t) continues from January to around May, although patterns there become irregular in April and May. From May into July (Fig. 6, parts E to G), a zone of heat storage evolves near the equator, with largest values in the West. Zonal contrasts are mitigated in August and September (Fig. 6, parts H and I), when a band of heat storage straddling the Equator between about 10°N and 10°S extends from the Americas into the Gulf of Guinea. From September to December (Fig. 6, parts I to L) the Q_t pattern in the equatorial Atlantic becomes irregular, while in the North Atlantic poleward of about 15°N heat storage gives way to heat depletion.

Figure 7 illustrates the phase lag in Q_t from the North to the South equatorial waters (zones 0–6°N versus 0–6°S), pointed out in relation to Figs. 3 and 4, as well as the broadly inverse annual cycles of Q_t in the western as compared to the eastern equatorial Atlantic described before by Merle (1980a, Fig. 5). Merle (1980a, 1985) reports that these variations in Q_t parallel annual cycle changes of thermocline depth resulting from seasonal variations in the surface wind field. Figure 7 serves to highlight the most prominent annual cycle

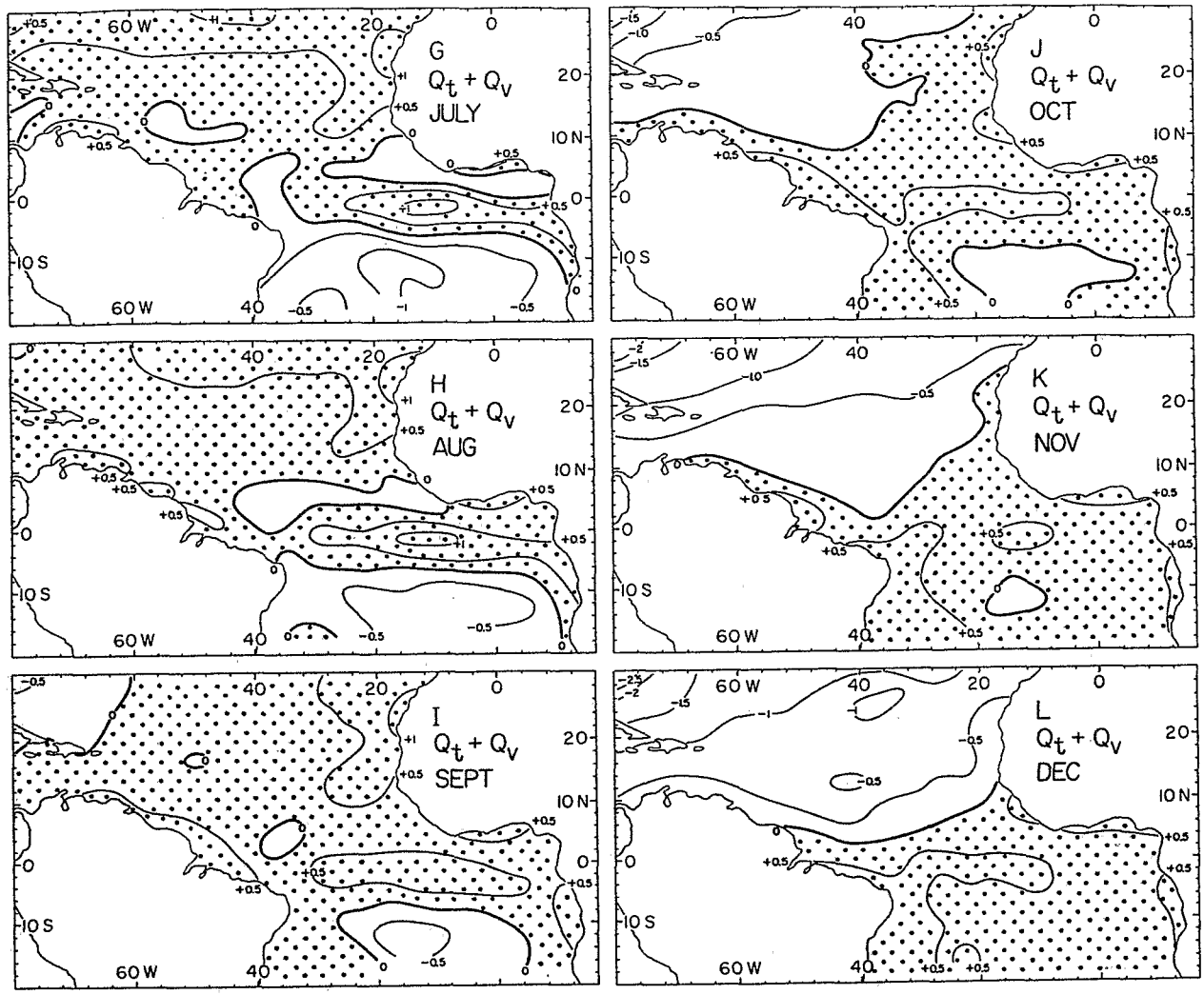

FIG. 5. (*Continued*)

characteristics of Q_t in the equatorial Atlantic contained in the details of the map sequence of Fig. 6.

A second (ii) system of annual cycle variations of Q_t prevails in the low latitude North Atlantic (about 0–15°N) and has likewise been referred to by Merle (1985) and Merle and Arnault (1985). Proceeding from around March to August (Fig. 6, parts C to H), there is an indication of a gradual northwestward displacement of a band of negative Q_t values, with positive Q_t values increasingly occupying the zone closer to the equator. A broadly reverse development is found from August to March (Fig. 6, parts H to L, and A to C). These shifts of the band of negative Q_t broadly parallel the seasonal migration of the confluence zone in the wind field over the tropical Atlantic (Hastenrath and Lamb, 1977, charts 16–21, 21–25, 14–16). It is here surmised that the positive curl of the wind stress associated with the surface wind discontinuity, through Ekman pumping, produces vertical displacements of the thermocline, which are in turn reflected in the spatial pattern of Q_t. Moreover it is noted that the North Equatorial Countercurrent (NECC) serves to advect heat from the warmer western to the cooler eastern portion of the ocean (Hastenrath and Lamb, 1978, charts 50–61), so that the northward displacement of the NECC from around April to August–September and its southward migration thereafter (Merle and Arnault, 1985) would contribute to the latitude shifts of the bands of heat storage/depletion illustrated in the map sequences of Fig. 6.

The maps of oceanic heat transport divergence Q_v (Fig. 8) exhibit patterns broadly complementary to those of Q_t (Fig. 6), because Q_v is obtained as difference between $(Q_t + Q_v)$ and Q_t (Figs. 5 and 6), and the variations of Q_t are much larger than those of $(Q_t + Q_v)$. This means that changes of oceanic heat content (Q_t)

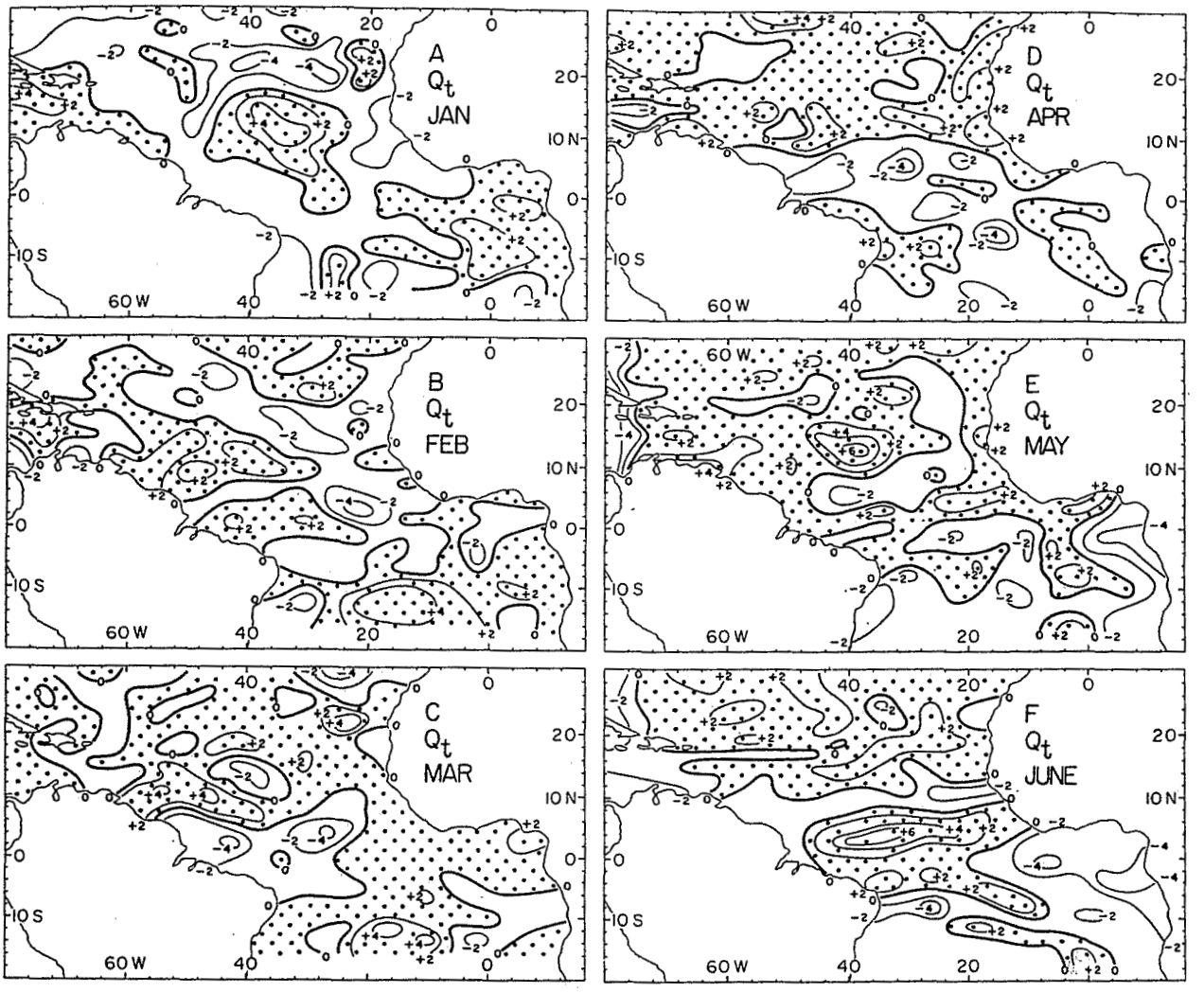

FIG. 6. Monthly maps of heat storage in the layer surface to 500 m, Q_{t500} for (A) January, (B) February, (C) March, (D) April, (E) May and (F) June. Figure 6 (continued) (G) July, (H) August, (I) September, (J) October, (K) November and (L) December. Quantities are in 10^2 W m^{-2}, zero line is heavy, and dot raster denotes positive areas.

in the equatorial Atlantic are primarily related to divergence/convergence of horizontal heat transport (Q_v), and not sea–air heat exchanges.

6. Summary and conclusions

The present analysis is based on a more voluminous collection of subsurface temperature soundings than previous studies covering the tropical Atlantic. The improved data base prompted the attempt to analyze spatial patterns of oceanic heat budget terms for all calendar months in addition to the evaluation of latitude-mean conditions. The net oceanic heat gain ($Q_t + Q_v$) follows in large part, but not exclusively, the annual cycle of insolation, with largest gain in the respective summer, and loss in the winter half-year. The Q_t exhibits a much larger annual range and more pronounced spatial gradients than ($Q_t + Q_v$). Poleward of about 15°N, the annual cycle of Q_t is similar to those of ($Q_t + Q_v$) and insolation, whereas temporal and spatial variations of Q_t are more complicated in the equatorial Atlantic (about 10°N–10°S). In the average over this latitude band, Q_t is largest negative (heat depletion) around March–May and largest positive (heat storage) around August–September. The latitude-average annual cycle of Q_v is broadly inverse to that of Q_t, because of the much smaller variations in ($Q_t + Q_v$).

The assessment of the latitude-mean conditions is complemented by the analysis of spatial patterns of heat budget terms and their annual cycle evolution. The calendar monthly maps of Q_t, and accordingly also of Q_v, are noisy, but serve the purpose of a first,

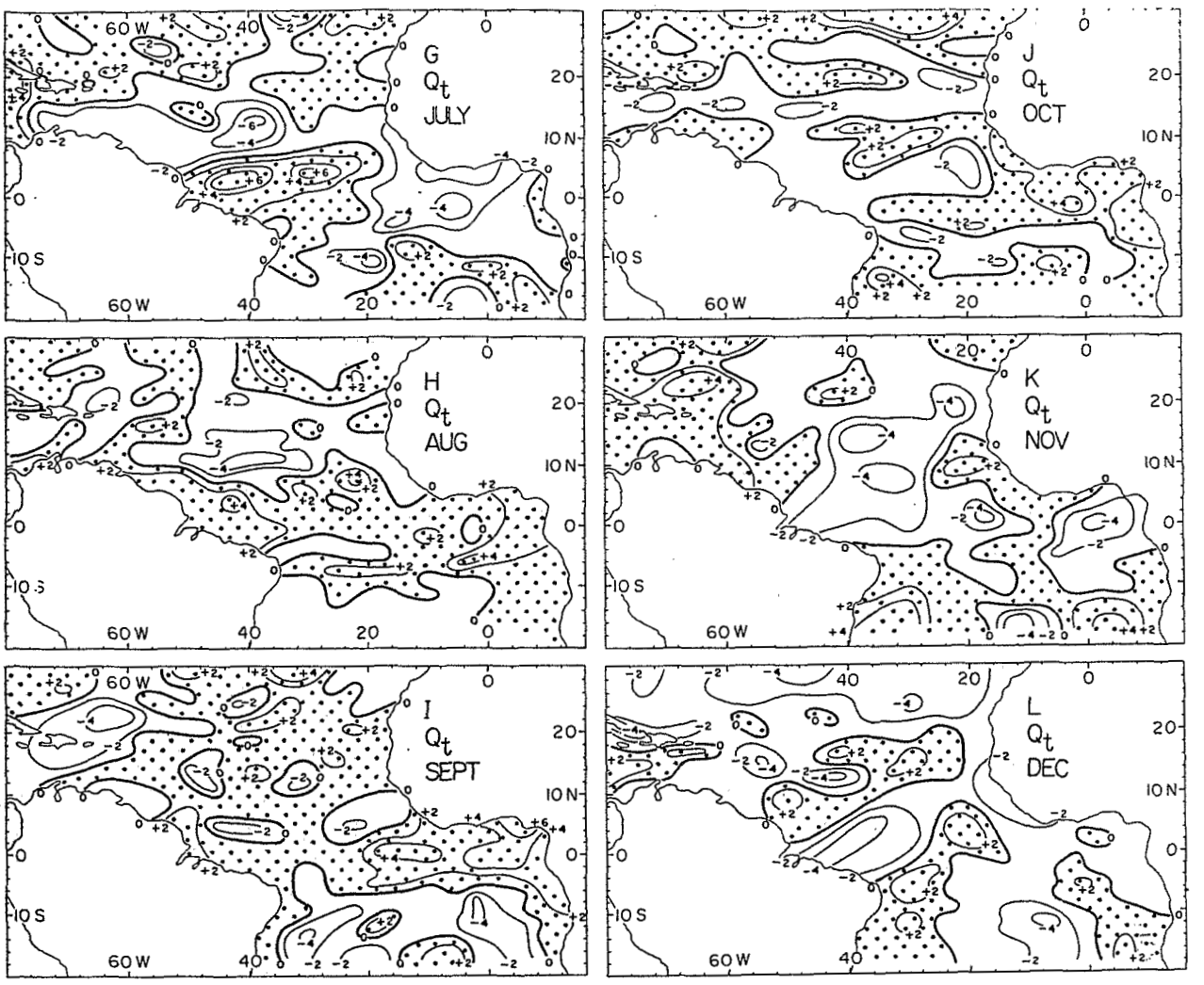

FIG. 6. (*Continued*)

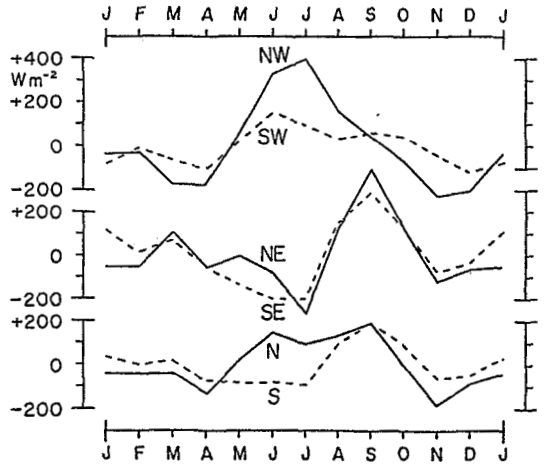

preliminary exploration. Two major systems of annual cycle changes of Q_t stand out in the low-latitude Atlantic with extrema around April and August, broadly concomitant with the annual cycle of the surface wind field.

(i) A teeter-totter variation of Q_t in the equatorial plane is apparent in the equatorial belt between about 10°S and 10°N, with heat depletion (negative Q_t) pre-

FIG. 7. Annual march of subsurface heat storage (Q_t) in the layer surface to 500 m in the equatorial Atlantic, in W m^{-2}. See Fig. 1 for delineation of areas. NW, solid line: 0–6°N, west of 20°W; SW, broken line: 0–6°S, west of 20°W; NE, solid line: 0–6°N, east of 20°W; SE, broken line: 0–6°S, east of 20°W; N, solid line: 0–6°N, zonal average; S, broken line: 0–6°S, zonal average.

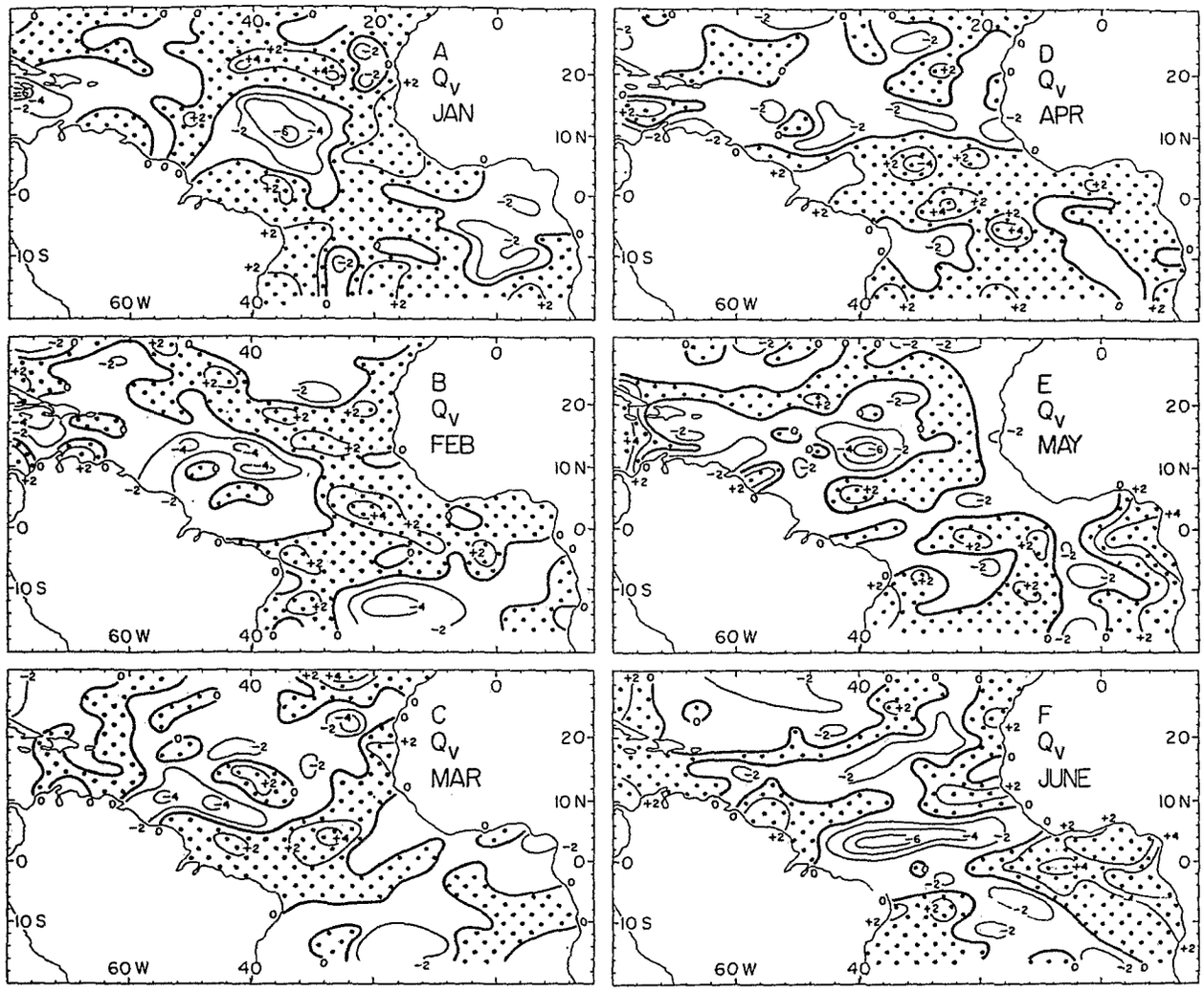

FIG. 8. Monthly maps of divergence of heat transport, calculated with reference to the 500 m level, $Q_{v500} = (Q_v + Q_t) - Q_{t500}$ for (A) January, (B) February, (C) March, (D) April, (E) May and (F) June. Figure 8 (continued) (G) July, (H) August, (I) September, (J) October, (K) November and (L) December. Quantities are in 10^2 W m^{-2}, zero line is heavy, and dot raster denotes positive areas.

vailing in the western equatorial Atlantic around March and April, and heat storage (positive Q_t) continuing in the Gulf of Guinea from January to around May. Zonal contrasts are mitigated in August and September, when heat storage prevails in the entire zone from the Americas to Africa. Patterns in the 10°S–10°N zone are somewhat irregular in April–May and September–December. The prevailing zonal seesaw in the heat budget pattern of the equatorial belt is associated with prominent changes in the subsurface thermal structure, namely a deepening of isothermal surfaces to the West from about May to July, with a concomitant shallowing in the Gulf of Guinea, and inverse developments after the height of the Northern summer. These annual cycle changes of subsurface thermal structure, which appear to be related to the seasonality of the surface wind field, will be analyzed in more detail in a forthcoming companion paper. However, earlier empirical studies (Merle, 1983; Merle and Arnault, 1985) and modeling experiments (Cane and Sarachik, 1981; Busalacchi and Picaut, 1983) suggest that the equatorial ocean can be approximated by two layers separated by the thermocline, and that remote wind-stress forcing over the western equatorial Atlantic can account for the zonal seesaw in thermocline depth.

(ii) Another prominent system of annual cycle variations of Q_t prevails in the equatorial North Atlantic, about 0–15°N. From around March to August, a band of negative Q_t values displaces northwestward, and positive Q_t values increasingly occupy the zone closer to the equator; inverse developments take place from August to around March. It is noteworthy that these annual cycle displacements of a band of negative Q_t broadly parallel the seasonal shifts in the position of

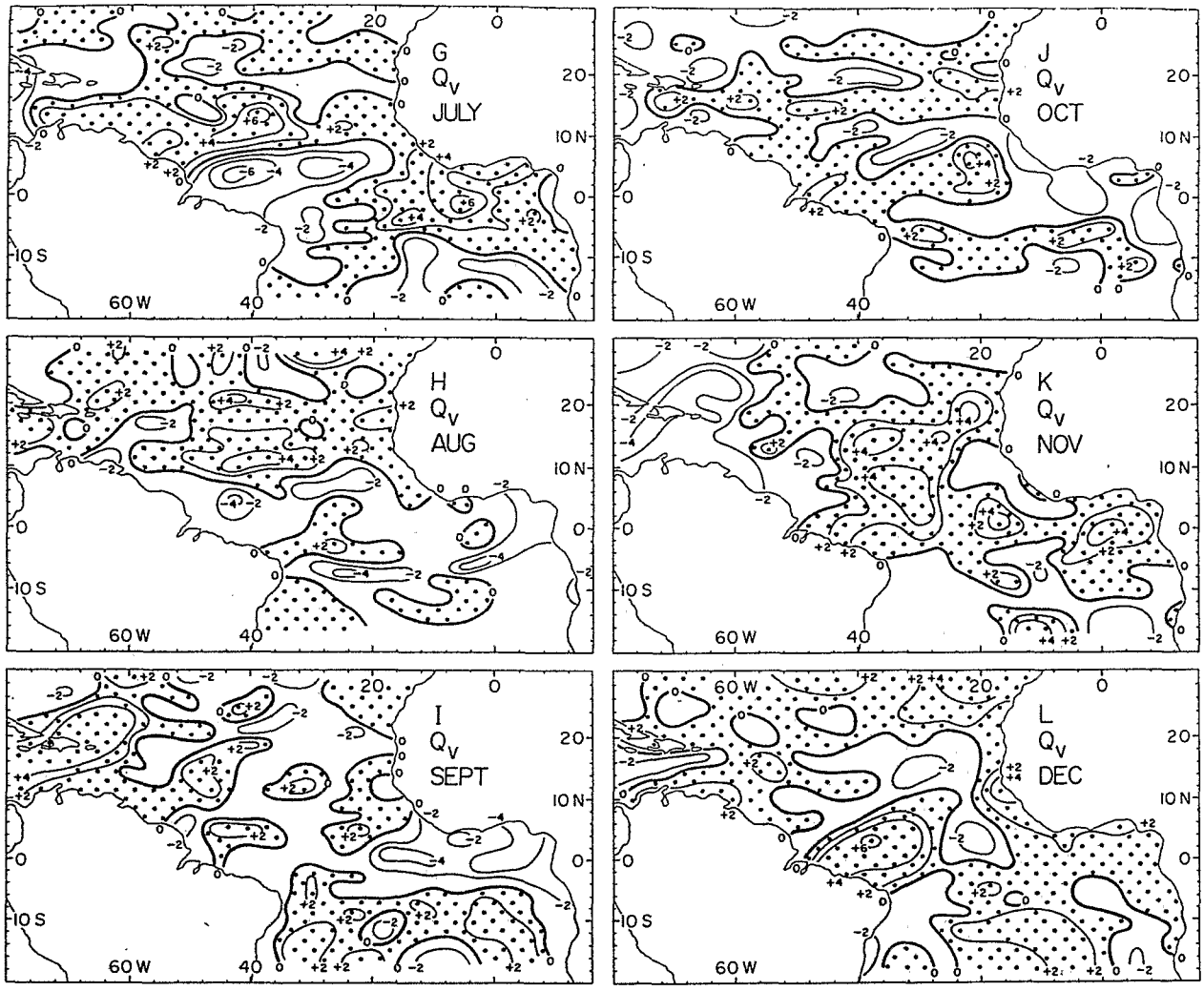

FIG. 8. (*Continued*)

the surface wind confluence over the tropical Atlantic, which in turn is associated with changes in the Ekman pumping. The effect of seasonal changes of Ekman pumping on the thermocline depth in this area has recently been discussed by Garzoli and Katz (1983).

The divergence of oceanic heat transport Q_v is obtained as a difference between the surface net oceanic heat gain ($Q_t + Q_v$) and the oceanic heat storage, and is accordingly fraught with the largest uncertainty. However, in the equatorial belt it has a magnitude comparable to, and spatial patterns broadly complementary to Q_t. Thus, changes of oceanic heat content are mainly related to divergence/convergence of horizontal heat transport. A remarkable feature of the equatorial Atlantic heat budget is the large annual and spatial variation of both heat storage and divergence of horizontal heat transport, neither of which follows the annual cycle of ($Q_t + Q_v$) and insolation. In contrast to the outer tropics and midlatitudes, the annual cycle of heat budget of the upper hydrosphere in the equatorial Atlantic appears to be primarily controlled by ocean dynamics. Regions of particular interest include the cold water regime immediately south of the eastern Atlantic equator and the realm of the "amphibious Intertropical Convergence Zone" of the Northern tropical Atlantic. The relation between oceanic heat storage/depletion, subsurface thermal structure, and lower atmospheric circulation, especially in these areas, is the object of our ongoing work.

Acknowledgments. S.H. acknowledges support through U.S. National Science Foundation Grants OCE81-20583 and OCE85-15009, and J.M. support by the Programme National d'Étude de la Dynamique du Climat through the FOCAL (Français Océan Climat

Atlantique ÉquatoriaL) Experiment. Carol Evans did the computer programming at the University of Wisconsin.

REFERENCES

Anonymous, 1981a: Seasonal equatorial Atlantic experiment. Lamont-Doherty Geological Observatory, Palisades, N.Y., 39 pp.

——, 1981b: Tropical Pacific upper ocean heat and mass budgets. Hawaii Institute of Geophysics Spec. Publ., 56 pp.

Barnett, T. P., 1981: On the nature and causes of large-scale thermal variability in the central North Pacific Ocean. *J. Phys. Oceanogr.*, **11**, 887–904.

Behringer, D. W., and H. Stommel, 1981: Annual heat gain of the tropical Atlantic from subsurface ocean data. *J. Phys. Oceanogr.*, **11**, 1383–1398.

Bennett, A. F., 1978: Poleward heat fluxes in Southern hemisphere oceans. *J. Phys. Oceanogr.*, **8**, 785–798.

Bryan, K., 1962: Measurements of meridional heat transport by ocean currents. *J. Geophys. Res.*, **67**, 3403–3414.

Bryden, H. L., and M. M. Hall, 1980: Heat transport by currents across 25°N latitude in the Atlantic Ocean. *Science*, **207**, 884–886.

Budyko, M. I., 1963: *Atlas of the Heat Balance of the Earth.* Kartfabrika Gosgeoltehizdata, Leningrad, 75 pp.

——, 1974: *Climate and Life. International Geophysics Series*, Vol. 18, Academic Press, 508 pp.

Bunker, A. F., 1976: Computations of surface energy flux and annual air–sea interaction cycles of the North Atlantic Ocean. *Mon. Wea. Rev.*, **104**, 1122–1140.

——, 1980: Trends of variables and energy fluxes over the Atlantic Ocean from 1948 to 1972. *Mon. Wea. Rev.*, **108**, 720–732.

——, and L. V. Worthington, 1976: Energy exchange charts of the North Atlantic Ocean. *Bull. Amer. Meteor. Soc.*, **57**, 670–678.

Busalacchi, A. J., and J. Picaut, 1983: Seasonal variability from a model of the tropical Atlantic Ocean. *J. Phys. Oceanogr.*, **13**, 1564–1588.

Cane, M., and E. Sarachik, 1981: The response of a linear baroclinic equatorial ocean to periodic forcing. *J. Mar. Res.*, **39**, 651–693.

Carissimo, B. C., A. H. Oort and T. H. Vonder Haar, 1985: On estimating the meridional energy transports in the atmosphere and ocean. *J. Phys. Oceanogr.*, **15**, 82–91.

Fu, L.-L., 1981: The general circulation and meridional heat transport of the subtropical South Atlantic determined by inverse methods. *J. Phys. Oceanogr.*, **11**, 1171–1193.

Garzoli, S. L., and E. J. Katz, 1983: The forced annual reversal of the Atlantic North Equatorial Countercurrent. *J. Phys. Oceanogr.*, **13**, 2082–2090.

Hastenrath, S., 1977: Relative role of atmosphere and ocean in the global heat budget: tropical Atlantic and eastern Pacific. *Quart. J. Roy. Meteor. Soc.*, **103**, 519–526.

——, 1978: Hemispheric asymmetry of the oceanic heat budget in the Equatorial Atlantic and Eastern Pacific. *Tellus*, **29**, 523–529.

——, 1980: Heat budget of tropical ocean and atmosphere. *J. Phys. Oceanogr.*, **10**, 159–170.

——, 1982: On meridional heat transports in the World ocean. *J. Phys. Oceanogr.*, **12**, 922–927.

——, and P. J. Lamb, 1977: *Climatic Atlas of the Tropical Atlantic and Eastern Pacific Oceans.* University of Wisconsin Press, 112 pp.

——, and ——, 1978: *Heat Budget Atlas of the Tropical Atlantic and Eastern Pacific Oceans.* University of Wisconsin Press, 104 pp.

——, and ——, 1979: *Climatic Atlas of the Indian Ocean. Part 1: The Surface Climate and Atmospheric Circulation, Part 2: The Oceanic Heat Budget.* University of Wisconsin Press, 116 and 110 pp.

Houghton, R. W., 1983: Seasonal variation of the subsurface thermal structure in the Gulf of Guinea. *J. Phys. Oceanogr.*, **13**, 2070–2081.

Lamb, P., 1981: Estimate of annual variation of Atlantic Ocean heat transport. *Nature*, **290**, 766–768.

——, 1984: On the mixed layer climatology of the North and tropical Atlantic. *Tellus*, **36A**, 292–305.

——, and A. F. Bunker, 1982: The annual march of the heat budget of the North and tropical Atlantic Oceans. *J. Phys. Oceanogr.*, **12**, 1388–1410.

Levitus, S., 1982: *Climatological Atlas of the World Ocean.* NOAA Prof. Paper No. 13, 173 pp.

Levitus, S., 1984: Annual cycle of temperature and heat storage in the World ocean. *J. Phys. Oceanogr.*, **14**, 727–746.

Merle, J., 1980a: Seasonal heat budget in the equatorial Atlantic Ocean. *J. Phys. Oceanogr.*, **10**, 464–469.

——, 1980b: Seasonal variation of heat storage in the tropical Atlantic Ocean. *Oceanol. Acta*, **3**, 455–463.

——, 1983: Seasonal variability of subsurface thermal structure in the tropical Atlantic Ocean. *Proc. 14th Annual Liege Colloq. on Ocean Hydrodynamics*, J. C. G. Nihoul, Ed., Elsevier, 31–50.

——, and S. Arnault, 1985: Seasonal variability of the surface dynamic topography in the tropical Atlantic Ocean. *J. Mar. Res.*, **43**, 267–288.

National Climate Program Office, NOAA, 1980: *National Climate Program, Five-Year Plan.* Washington, D.C., 101 pp.

Niiler, P. P., and W. J. Richardson, 1973: Seasonal variability of the Florida Current. *J. Mar. Res.*, **31**, 144–167.

Oort, A. H., and T. H. Vonder Haar, 1976: On the observed annual cycle in the ocean–atmosphere heat balance over the Northern hemisphere. *J. Phys. Oceanogr.*, **6**, 781–799.

Reed, R. K., 1983: Heat fluxes over the Eastern tropical Pacific and aspects of the 1972 El Niño. *J. Geophys. Res.*, **88**, 9627–9638.

Robinson, M., R. Bauer and E. Schroeder, 1979: *Atlas of North Atlantic–Indian Ocean Monthly Mean Temperatures and Mean Salinities of the Surface Layer.* Naval Oceanographic Office, NOO RP-18, 234 pp.

Roemmich, D., 1980: Estimation of meridional heat flux in the North Atlantic Ocean by inverse methods. *J. Phys. Oceanogr.*, **10**, 1972–1983.

Weare, B. C., P. T. Strub and M. D. Samual, 1981: Annual mean surface heat fluxes in the tropical Pacific Ocean. *J. Phys. Oceanogr.*, **11**, 705–717.

World Meteorological Organization, 1980: Outline plan and basis for the World Climate Programme, 1980–83. Geneva, WMO-No. 540, 64 pp.

World Meteorological Organization-ICSU, 1980: Report of the first session of the Joint Scientific Committee, Amsterdam, March–April 1980.

——, 1983: Large-scale oceanographic experiments in the WCRP. WCRP Publ. Ser., No. 1, 2 vols., 121 and 544 pp.

Wunsch, C., 1980: Meridional heat flux in the North Atlantic Ocean. *Proc. Natl. Acad. Sci., USA*, **77**, 5043–5047.

——, D. Hu and B. Grant, 1983: Mass, heat, salt, and nutrient fluxes in the South Pacific Ocean. *J. Phys. Oceanogr.*, **13**, 725–753.

Wyrtki, K., 1965: The average annual heat balance of the North Pacific Ocean and its relation to ocean circulation. *J. Geophys. Res.*, **70**, 4547–4559.

——, 1966: Seasonal variation of heat exchange and surface temperature in the North Pacific Ocean. Hawaii Institute of Geophysics, Rep. H16-66-3.

——, and L. Uhrich, 1982: On the accuracy of heat storage computations. *J. Phys. Oceanogr.*, **12**, 1411–1416.

Reprinted from JOURNAL OF PHYSICAL OCEANOGRAPHY, Vol. 16, No. 4, April 1986
American Meteorological Society

The Annual March of Heat Storage and Export in the Tropical Atlantic Ocean

STEFAN HASTENRATH

JACQUES MERLE